Modeling and Joint Mitigation of TX and RX Nonlinearity Induced Receiver Desensitization

Adnan Kiayani, *Member, IEEE,* Lauri Anttila, *Member, IEEE,* Marko Kosunen, *Member, IEEE,* Kari Stadius, *Member, IEEE,* Jussi Ryynänen, *Member, IEEE,* and Mikko Valkama, *Senior Member, IEEE*

***Abstract*—In this article, we provide detailed modeling of the spurious intermodulation distortion (IMD) products appearing in the own receiver (RX) operating band as a result of coexisting transmitter (TX) and RX nonlinearities with noncontiguous carrier aggregation (CA) transmissions. Furthermore, an efficient digital front-end signal processing technique is proposed, which can flexibly mitigate the resulting receiver in-band self-interference caused either by individual or simultaneously coexisting TX and RX nonlinearities. The technique is based on accurately estimating the effective leakage channel that models the nonlinearities of the transmitter and receiver chains and the duplexer filters characteristics. In the parameter estimation stage, an observation receiver chain is adopted for separately estimating the TX passband leakage response, which facilitates efficient joint estimation and regeneration of the TX and RX induced self-interference. In the online digital cancellation, the actual transmit data is used in conjunction with the estimated channel responses to generate a replica of the overall nonlinear self-interference, which is subsequently suppressed by subtracting it from the actual observation. In general, the proposed technique can efficiently estimate and suppress the self-interference at arbitrary spurious sub-bands located at the RX band. The performance evaluations with comprehensive numerical simulations and practical RF measurements indicate highly accurate and efficient operation, with up to 28 dB of measured self-interference suppression.**

***Index Terms*—Carrier aggregation, digital cancellation, desensitization, flexible duplexing, frequency division duplexing, intermodulation distortion, low noise amplifier, LTE-Advanced, power amplifier, self-interference, spurious emissions, 5G.**

I. Introduction

CARRIER AGGREGATION (CA) is a key technology in the Third Generation Partnership Project (3GPP) Long Term Evolution (LTE)-Advanced network to support wider transmission bandwidths and higher data rates [1], [2]. The CA technique permits flexible aggregation of LTE carriers, commonly called Component Carriers (CCs), that can be located within the same operating band (intraband CA) or in different operating bands (interband CA). Moreover, aggregated carriers can have different bandwidths and may also be noncontiguously located even in the intraband case [1] - [4].

This work was funded by the Academy of Finland under the projects #284694, #288670, #301820, and #304147. The work was also supported by the Linz Center of Mechatronics (LCM) in the framework of the COMET-K2 program of the Austrian Federal government, and Nokia Networks.

A. Kiayani, L. Anttila, and M. Valkama are with the Department of Electronics and Communications Engineering, Tampere University of Technology, FI-33101 Tampere, Finland (e-mail: adnan.kiayani@tut.fi, lauri.anttila@tut.fi, mikko.e.valkama@tut.fi).

M. Kosunen, K. Stadius, and J. Ryynänen are with the Department of Electronics and Nanoengineering, Aalto University, FI-00076 Espoo, Finland.

From the radio frequency (RF) implementation perspective, the adoption of CA technology poses major challenges, in particular related to transceiver linearity. The Frequency Division Duplex (FDD) mode of LTE-Advanced is particularly challenging, where an RF duplexer is used to enable simultaneous operation of the transmitter (TX) and the receiver (RX). As the CA technology tends to reduce the duplex distance, especially when configured in the noncontiguous aggregation mode, achieving sufficient TX-RX isolation through a duplexer becomes increasingly difficult [5], [6]. As a result, the receiver is exposed to the unwanted self-interference created by the nonlinearities of the RF components in the TX and RX chains, and possibly leading to own RX (self-)desensitization. This is depicted in Fig. 1 for the practical case of a dual-carrier intraband noncontiguous CA transmission scenario employing a nonlinear PA and LNA in the TX and RX chains, respectively, where the resulting TX and RX nonlinearity-induced spurious intermodulation distortion (IMD) products are coexisting and some of them appear in the RX operating band.

To prevent the own RX desensitization, a straightforward approach is to improve the stopband response of duplexer filters; however, this may result in increased passband insertion loss and duplexer cost. Other options are to reduce the transmit power, i.e., PA back-off, such that the levels of transmitter leakage signals are reduced, or to deploy more linear components, or alternatively increase the duplex distance. These solutions are, however, not very tempting as they will reduce the coverage and power efficiency, increase costs and size of the devices, and/or reduce the flexibility in the RF spectrum use.

Recently, digital cancellation methods have been extensively investigated to reduce the harmful impacts of TX leakage signals, and to reduce the RX desensitization [7] - [18]. The works in [7] - [8] consider the cancellation of second-order IMD (IMD2) caused by the transmitter passband signal leaking into the RX chain and the RX mixer nonlinearity, while completely neglecting the TX PA nonlinearity and the associated receiver in-band self-interference. The authors in [9] considered specific TX nonlinearities, but only pursue the cancellation of RX nonlinearity-induced IMD2 products. On the other hand, the works in [10] - [16] consider only the TX nonlinearity-induced distortion at the own RX band while assuming an ideal linear RX. Recently, in [17] and [18], the authors proposed digital cancellation solutions for the self-interference in a specific receiver band caused by the passive components in the transceiver RF front-end, such as nonlinear antenna switches, duplexer, and diplexer, in the interband

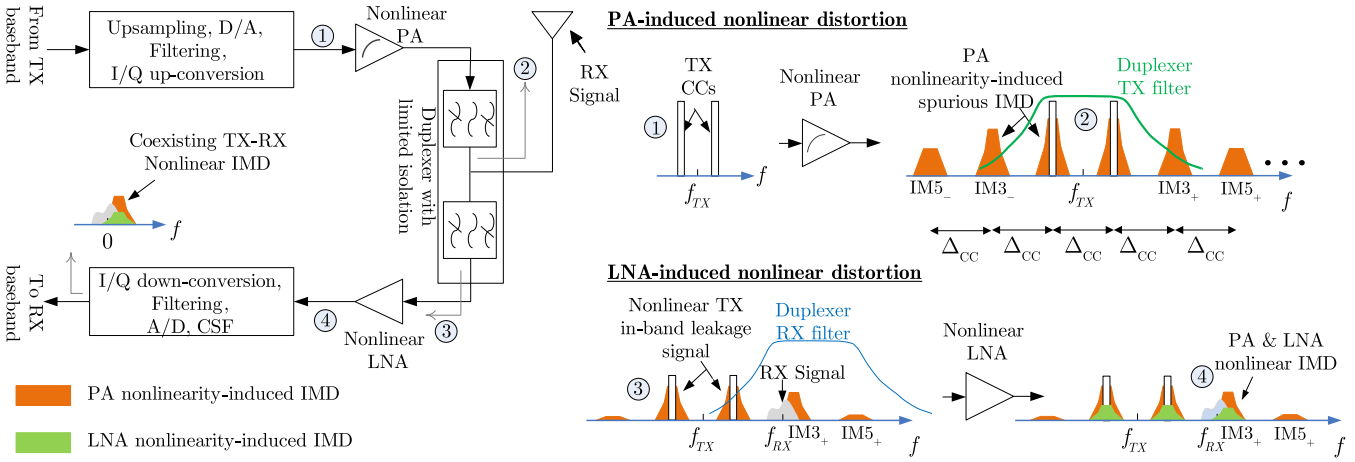

Fig. 1. Illustration of the spurious IMD products created by a nonlinear PA and a nonlinear LNA, hitting own receiver band in the CA transmission with two noncontiguous CCs. The center frequency of the receiver, f_{RX}, is assumed to be in close proximity to the upper third-order intermodulation sub-band (IM3_+).

CA transmission scenario, where each LTE operating band is assumed to have a separate radio transmitter and receiver. Therefore, the existing works are clearly limited and lack the treatment, modeling, and suppression of the receiver in-band self-interference caused by the coexisting TX and RX nonlinearities in the FDD transceivers supporting intraband noncontiguous CA.

In this paper, we address the transmitter and receiver linearity challenges of FDD transceivers that transmit noncontiguous intraband CA waveforms, focusing specifically on the spurious IMD products appearing in the operating band of the own receiver, due to a nonlinear TX PA, finite isolation duplexer filter, and a nonlinear RX LNA, all coexisting simultaneously. A novel flexible and low-complexity digital estimation-cancellation solution for effectively mitigating the resulting nonlinear self-interference at specific sub-bands, that can potentially be present in the receiver operating band, is also proposed. The nonlinear characteristics of the TX and RX front-end components and the duplexer filters responses are all assumed unknown, and are modeled as an effective leakage channel whose coefficients are estimated. An efficient method is then developed building on the established signal models, which operates in the transceiver digital front-end and is capable of regenerating and suppressing the receiver in-band self-interference when coexisting TX-RX nonlinearities are present. The efficiency and performance of the proposed solution is quantified and demonstrated with simulations and true RF measurements using commercial LTE/LTE-Advanced PA, duplexer, and LNA modules, covering both the user equipment (UE) and the base station (BS) sides. The obtained results suggest that the proposed technique can achieve excellent suppression of the self-interference, therefore relaxing the duplexer isolation and the duplex distance requirements, and also potentially relaxing the linearity requirements of the transceiver RF components. This type of advanced self-interference cancellation techniques are likely to play a key role also in 5G/new radio (NR) developments [19], where flexible duplexing at both paired and unpaired spectra is one central element.

The rest of the article is structured as follows. The FDD transceiver implementation challenges in employing noncontiguous CA waveforms, and the resulting degradation in the RX performance due to spurious IMD products are demonstrated through transceiver system calculations in Section II. Section III formulates the essential signal models describing the TX and RX nonlinearity-induced spurious IMD products in the receiver band. Stemming from this modeling, Section IV then describes the proposed self-interference regeneration and cancellation technique, together with the needed parameter estimation methods. The complexity analysis of the proposed technique is presented in Section V, and the practical implementation aspects of the proposed technique are also reviewed. Finally, Sections V and VI report and analyze the simulation and practical RF measurement results, respectively, and Section VII presents conclusions. The signal models and basis functions for the spurious IMD products at higher-than third-order IM (IM3) sub-bands are presented in the Appendix.

II. Considered FDD Transceiver Implementation Challenges with Noncontiguous CA Transmission

In general, the contiguous CA transmission has many implementation benefits in terms of cost, complexity, and power consumption as compared to the noncontiguous CA transmission [3], [20]. However, due to spectrum licensing for LTE-Advanced systems, it is difficult to allocate a large contiguous spectrum to an individual operator. Thus, in order to improve the overall radio spectrum utilization, noncontiguous CA is an intriguing approach. We also focus in this paper on the noncontiguous CA transmission, assuming the practical case of two intraband CCs, and address the associated TX and RX RF linearity challenges.

A. Transceiver Architecture and Sources of Self-Interference

In general, the implementation of a radio transceiver is heavily influenced by the adopted CA mode. On the TX side,

combining the CCs before the PA and thus using a single PA for transmission results in a better power efficiency [3], [20]. Note that the reference transmitter architecture for intraband noncontiguous CA in 3GPP specifications also assumes a single PA in the TX chain, for both UE and BS sides. However, with such an implementation, the PA nonlinearity produces strong spurious IMD products of the CCs that are not only located around the main carriers, causing classical spectral regrowth, but also at specific IM sub-bands that are located at integer multiples of the CC spacing away from the component carriers, as shown in Fig. 1. Moreover, higher-order IMD products are also typically present at these IM sub-band, while some of the IM sub-bands can then appear in the RX operating band. The powers of these unwanted IMD products depend on the TX power, PA nonlinearity characteristics, and if interpreted on the RX side, also on the duplexer TX filter characteristics. The duplexer TX filter alone may not sufficiently suppress the unwanted TX emissions at RX band, in particular when emphasizing power efficiency and increased spectrum flexibility, hence causing RX desensitization.

Another central challenge in employing noncontiguous transmissions is the TX passband signal leaking into the receiver due to insufficient attenuation of the duplexer RX filter for the transmitter passband frequencies, thus imposing stringent RX LNA linearity requirements. Due to the nonlinearity of RX LNA, spurious IMD products of the TX passband leakage signal are produced which, in practice, coexist with the PA nonlinearity-induced IMD products, as shown in Fig. 1. The strength of the LNA-induced IMD products depends on the LNA linearity, typically characterized by the third-order intercept point (IIP3), TX power, and the duplexer attenuation for TX passband, and can also be substantial with state-of-the-art LNA and duplexer modules as we demonstrate in the following subsection.

B. Example Transceiver System Calculations

In this subsection, we carry out example system calculations assuming realistic LTE/LTE-Advanced UE and BS parameters, in order to demonstrate and quantify the relative strengths of the PA and LNA nonlinearity-induced IMD products appearing in the own RX operating band. As a practical example, LTE Band 25 is assumed as the operating band with dual-carrier intraband CA transmission of 5 MHz CCs assigned to TX operating band edges. With such a carrier placement, the duplex distance reduces to only 20 MHz, hence reflecting a challenging duplexer isolation scenario. The transmitter generates a powerful transmit signal with an average transmit power denoted here by P_{TX}, and the receiver is protected against the TX emissions through a finite isolation duplexer, whose attenuation is denoted by A_{DUP}.

In order to avoid degrading the RX performance, the TX and RX nonlinearity-induced distortion products at the receiver band are required to be lower than the effective thermal noise floor, in particular when receiving signals close to the reference sensitivity level. The system parameters and the resulting receiver in-band self-interference due to nonlinear IMD products are presented in Table I. For true comparison, the power values in the table are corrected to map the power to dBm/5 MHz scale, which corresponds to the receiver in-band power. Furthermore, for the UE case, it is assumed that the TX emissions at the RX band satisfy the general spurious emissions limit defined in the 3GPP specifications, i.e., -30 dBm/1 MHz [4], being then further suppressed by the duplexer. On the other hand, in the BS case, we adopt the maximum spurious emissions limit specified by 3GPP to protect a wide area BS receiver, i.e., -86 dBm/1 MHz [22], which is measured at the antenna connector. In addition, since the power at the IM3 sub-band is typically 10 dB less than the total power of the third-order IMD products, being divided between the main CCs as well as at the negative and positive IM3 sub-bands, we have subtracted 10 dB from the total power when calculating the LNA-induced third-order IMD component located at the positive IM3 sub-band.

TABLE I
EXAMPLE SYSTEM PARAMETERS AND CALCULATED RECEIVER IN-BAND SELF-INTERFERENCE POWERS DUE TO THE NONLINEARITIES OF THE TRANSMITTER AND RECEIVER CHAINS AND LIMITED DUPLEXER ATTENUATION, ASSUMING 5 MHZ CCS.

Parameter	Unit	Value	
		UE	BS
TX power (P_{TX})	dBm	$+23$	$+46$
Duplexer isolation (A_{DUP})	dB	50	70
TX passband leakage signal power $P_{\mathrm{TxL}} = P_{\mathrm{TX}} - A_{\mathrm{DUP}}$	dBm	-27	-24
TX spurious emissions at RX band $P_{\mathrm{PA}}^{\mathrm{IMD}}$	dBm	-73	-79
RX noise figure (NF)	dB	9	4
Thermal noise level $P_{\mathrm{Noise}} = -174 + \mathrm{NF} + 67$	dBm	-98	-103
RX reference sensitivity level (P_{RefSens})	dBm	-96.5	-101.6
Degradation in RX sensitivity due to TX IMD leakage $P_{\mathrm{PA}}^{\mathrm{IMD}} - P_{\mathrm{Noise}}$	**dB**	**25**	**24**
LNA out-of-band IIP3 (IIP3)	dBm	-5	0
LNA-induced third-order IMD at IM3 sub-band, referenced to LNA input $P_{\mathrm{LNA}}^{\mathrm{IMD}} = 3P_{\mathrm{TxL}} - 2\mathrm{IIP3}$	dBm	-85.77	-86.77
Degradation in RX sensitivity due to RX IMD $P_{\mathrm{LNA}}^{\mathrm{IMD}} - P_{\mathrm{Noise}}$	**dB**	**12.23**	**16.23**

It can be observed from Table I that both the TX-induced IMD and the RX-induced IMD are clearly above the thermal noise floor, and are also stronger than the desired RX signal when it is received at the reference sensitivity level.

In general, these system calculations reflect and demonstrate the clear challenges related to the TX and RX-induced nonlinear distortion at the own RX band, and thereon motivate towards the development of advanced self-interference cancellation solutions. Similar observations have recently been made in 3GPP, see, e.g., [5] and [6]. In the next section, the behavioral modeling for the spurious IMD products that can potentially be present in the RX band is carried out, and

building on that, a novel digital estimation and cancellation solution is proposed.

III. RX In-band Self-Interference Modeling in CA FDD Transceivers

We begin by formulating the fundamental discrete-time baseband equivalent signal models describing the spurious IMD stemming from the nonlinear TX-RX chain components, and the resulting receiver in-band self-interference. On the TX side, a nonlinear PA with memory is adopted, followed by a duplexer with finite stopband attenuation, while a nonlinear LNA is assumed in the RX chain. For practical purposes and notational simplicity, we concentrate on intraband non-contiguous CA transmission with two CCs; nevertheless, the proposed modeling can be easily generalized to support more than two carriers by always clustering the CCs into two groups. Furthermore, in this section, it is assumed that the positive IM3 sub-band of the transmit signal overlaps with the RX operating band and therefore causes interference to the desired RX signal. The exact signal models of the higher-than third-order IM sub-bands that can potentially also appear at the RX band are provided in the Appendix.

Now, consider a generic intraband noncontiguous CA FDD transceiver, shown in Fig. 2, with two CCs that are separated by $\Delta_{CC} = 2\omega_{\rm IF}$. The baseband signals of individual CCs are denoted by $x_1[n]$ and $x_2[n]$, and the composite baseband equivalent transmit signal is then written as

$$x[n] = x_1[n]e^{j\omega_{\rm IF}n} + x_2[n]e^{-j\omega_{\rm IF}n} \tag{1}$$

where $\omega_{\rm IF}$ and $-\omega_{\rm IF}$ denote the digital intermediate frequencies (IFs) of the individual CCs. The baseband equivalent PA output signal reads

$$x_{\rm PA}[n] = \sum_{\substack{p=1\\ p\ odd}}^{P} f_p^{\rm PA}[n] \star |x[n]|^{p-1}\, x[n] \tag{2}$$

where we utilize the widely adopted parallel Hammerstein (PH) PA model, which has been shown to be accurate in modeling the nonlinearity of a wideband PA with memory [14], [24], [26]. In the above equation, P is the highest nonlinearity order, $f_p^{\rm PA}[n]$ is the baseband equivalent impulse response of the $p^{th}-$order PH branch filter, and $\star$ is the convolution operator. The nonlinearity of the PA generates spurious IMD products of the CCs, resulting in the classical spectral regrowth around the main CCs, as well as the unwanted IMD products that are located at the positive and negative IM sub-bands.

The transmit signal then travels from the duplexer towards the antenna, but due to limited duplexer filters stopband attenuation, it also leaks partly towards the receiver. At the receiver input, through straight-forward manipulations, the TX leakage signal can be expressed as

$$\begin{aligned} x_{\rm TxL}[n] &= \left(h_{\rm D}[n] \star x_{\rm PA}[n]\right) e^{-j\omega_{\rm D}n} \\ &= x_{\rm TX}^{\rm passband}[n]e^{-j\omega_{\rm D}n} + x_{\rm TX}^{\rm OOB}[n]e^{-j\Delta\omega n} \end{aligned} \tag{3}$$

where

$$h_{\rm D}[n] = \left(h_{\rm D}^{\rm RX}[n]e^{j\omega_{\rm D}n}\right) \star h_{\rm D}^{\rm TX}[n] \tag{4}$$

denotes the effective baseband duplexer filter response, with $h_{\rm D}^{\rm TX}[n]$ and $h_{\rm D}^{\rm RX}[n]$ representing the equivalent baseband impulse responses of the bandpass duplexer TX and RX filters, respectively. Furthermore, $x_{\rm TX}^{\rm passband}[n]$ and $x_{\rm TX}^{\rm OOB}[n]$ in (3) denote the TX passband signal and the TX OOB signal leaking into the RX chain, respectively. We will discuss in details these two components of the TX signal in the forthcoming subsection.

In the above expressions, $\omega_{\rm D} = 2\pi(f_{\rm RX} - f_{\rm TX})/f_s$ denotes the normalized duplex distance between the TX and RX operating frequencies. For completeness of modeling, it is also assumed that there exists a small frequency separation between a specific spurious IM sub-band located at the own RX band and the desired RX signal, denoted by $\Delta\omega$. For example, when the IM3$_+$ sub-band is present in close proximity of the RX band then $\Delta\omega = \omega_{\rm D} - 3\omega_{\rm IF}$.

A. Transmitter Passband Leakage Signal

The TX passband signal leaking into the RX, denoted by $x_{\rm TX}^{\rm passband}[n]$ in (3), refers to the portion of the transmit signal that is within the passband of the duplexer TX filter, but is then suppressed to a certain extent by the duplexer RX filter. It can be obtained through direct substitution of (1) and (2) in (3), which yields

$$x_{\rm TX}^{\rm passband}[n] = h_{\rm D}[n] \star \sum_{\substack{p=1\\ p\ odd}}^{P} \begin{pmatrix} f_p^{\rm PA,IF_+}[n] \star \psi_p^{\rm PA,IF_+}[n] + \\ f_p^{\rm PA,IF_-}[n] \star \psi_p^{\rm PA,IF_-}[n] \end{pmatrix}. \tag{5}$$

Here, $\psi_p^{\rm PA,IF_\pm}[n]$ denote the static nonlinear (SNL) basis functions for the positive and negative IF sub-bands, and $f_p^{\rm PA,IF_\pm}[n]$ denote the baseband equivalent responses of the p^{th}-order PH branch filter $f_p^{\rm PA}[n]$ around the IF sub-bands. These filters are formally defined as

$$f_p^{\rm PA,IF_\pm}[n] = h^{\rm LPF}[n] \star (f_p^{\rm PA}[n]e^{\mp j\omega_{\rm IF}n}), \tag{6}$$

where $h^{\rm LPF}[n]$ refers to a lowpass filter impulse reponse whose passband width is equal to $P-$times the bandwidth of the CC. The basis functions $\psi_p^{\rm PA,IF_+}[n]$, considering up to ninth-order distortion products in the TX band, can be shown to read

$$\begin{aligned} \psi_1^{\rm PA,IF_+}[n] &= x_1[n]e^{j\omega_{\rm IF}n} \\ \psi_3^{\rm PA,IF_+}[n] &= x_1[n] \times \left(|x_1[n]|^2 + 2\,|x_2[n]|^2\right) e^{j\omega_{\rm IF}n} \\ \psi_5^{\rm PA,IF_+}[n] &= x_1[n] \times \begin{pmatrix} |x_1[n]|^4 + 3\,|x_2[n]|^4 + \\ 6\,|x_1[n]|^2\,|x_2[n]|^2 \end{pmatrix} e^{j\omega_{\rm IF}n} \\ \psi_7^{\rm PA,IF_+}[n] &= x_1[n] \times \begin{pmatrix} |x_1[n]|^6 + 4\,|x_2[n]|^6 + \\ 12\,|x_1[n]|^4\,|x_2[n]|^2 + \\ 18\,|x_1[n]|^2\,|x_2[n]|^4 \end{pmatrix} e^{j\omega_{\rm IF}n} \\ \psi_9^{\rm PA,IF_+}[n] &= x_1[n] \times \begin{pmatrix} |x_1[n]|^8 + 5\,|x_2[n]|^8 + \\ 20\,|x_1[n]|^6\,|x_2[n]|^2 + \\ 40\,|x_1[n]|^2\,|x_2[n]|^6 + \\ 60\,|x_1[n]|^4\,|x_2[n]|^4 \end{pmatrix} e^{j\omega_{\rm IF}n}, \end{aligned} \tag{7}$$

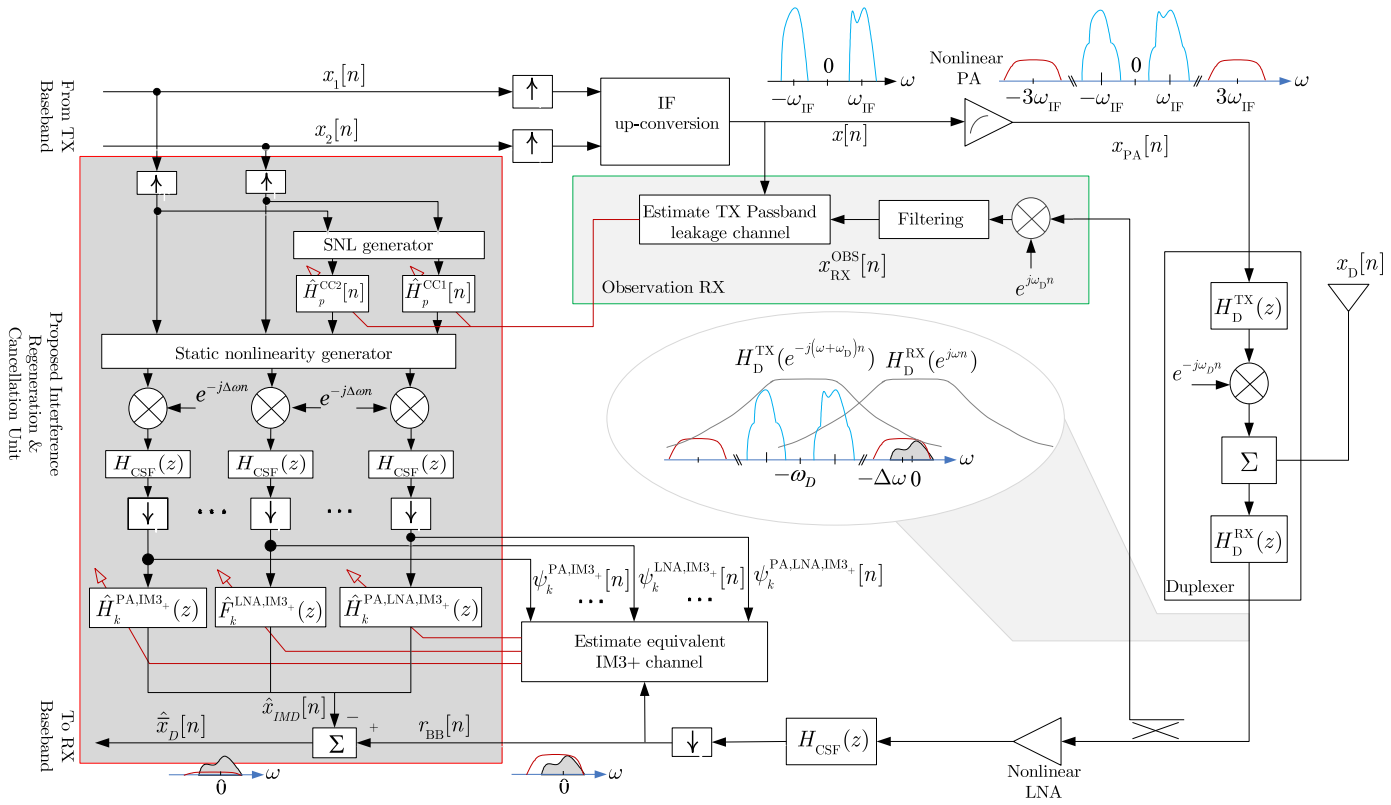

Fig. 2. A block diagram of an intraband CA FDD transceiver with two CCs, where baseband equivalent discrete-time signal and component models are utilized. The proposed architecture for the in-band self-interference regeneration and suppression is also shown, which is operating in the transceiver's digital front-end. The symbols ↑ and ↓ denote the upsampling and downsampling operations, respectively.

while $\psi_p^{\mathrm{PA,IF_-}}[n]$ can be easily obtained from (7) by interchanging $x_1[n]$ and $x_2[n]$ and substituting $-\omega_{\mathrm{IF}}$ for ω_{IF}.

B. TX Out-of-Band Leakage Signal

In the context of noncontiguous transmission, the TX OOB leakage signal refers to the spurious IMD products that are outside the transmitter operating band. Depending on the CC spacing and the locations of the TX and RX operating frequency bands, some of these spurious components may appear directly in the own RX band. Due to limited isolation of the duplexer TX filter, the unwanted IMD components are not fully suppressed, hence potentially causing the desensitization of own receiver.

We assume here a concrete example case where the IM3$_+$ sub-band appears in the RX operating band. However, the analysis is further extended in the Appendix to include higher-order IM sub-bands that can also lie in the RX band. For the spurious IM3$_+$ sub-band, the OOB leakage component in (3) can be expressed as

$$x_{\mathrm{TX}}^{\mathrm{OOB,IM3_+}}[n] = h_{\mathrm{D}}[n] \star \left(\sum_{\substack{p=3 \\ p\ odd}}^{P} f_p^{\mathrm{PA,IM3_+}}[n] \star \psi_p^{\mathrm{PA,IM3_+}}[n] \right), \tag{8}$$

where $\psi_p^{\mathrm{PA,IM3_+}}[n]$ are the SNL basis functions at the IM3$_+$ sub-band. Assuming an eleventh-order PA model as a practical example, the different orders of SNL basis functions, modeling the IMD products at the IM3$_+$ sub-band, are given in (9), where $f_p^{\mathrm{PA,IM3_+}}[n] = h^{\mathrm{LPF}}[n] \star (f_p^{\mathrm{PA}}[n] e^{-j3\omega_{\mathrm{IF}} n})$ denote the unknown baseband equivalent responses of $f_p^{\mathrm{PA}}[n]$ at the positive IM3 sub-band.

$$\begin{aligned}
\psi_3^{\mathrm{PA,IM3_+}}[n] &= x_1^2[n] x_2^*[n] \\
\psi_5^{\mathrm{PA,IM3_+}}[n] &= \psi_3^{\mathrm{PA,IM3_+}}[n] \times \left(2|x_1[n]|^2 + 3|x_2[n]|^2 \right) \\
\psi_7^{\mathrm{PA,IM3_+}}[n] &= \psi_3^{\mathrm{PA,IM3_+}}[n] \times \begin{pmatrix} 3|x_1[n]|^4 + 6|x_2[n]|^4 + \\ 12|x_1[n]|^2 |x_2[n]|^2 \end{pmatrix} \\
\psi_9^{\mathrm{PA,IM3_+}}[n] &= \psi_3^{\mathrm{PA,IM3_+}}[n] \times \begin{pmatrix} 4|x_1[n]|^6 + 10|x_2[n]|^6 + \\ 30|x_1[n]|^4 |x_2[n]|^2 + \\ 40|x_1[n]|^2 |x_2[n]|^4 \end{pmatrix} \\
\psi_{11}^{\mathrm{PA,IM3_+}}[n] &= \psi_3^{\mathrm{PA,IM3_+}}[n] \times \begin{pmatrix} 5|x_1[n]|^8 + 15|x_2[n]|^8 + \\ 60|x_1[n]|^6 |x_2[n]|^2 + \\ 100|x_1[n]|^2 |x_2[n]|^6 + \\ 150|x_1[n]|^4 |x_2[n]|^4 \end{pmatrix}.
\end{aligned} \tag{9}$$

C. Contributions of the RX Nonlinearity

The signal at the receiver input is composed of the TX leakage signals, described above, as well as the desired received signal and the thermal noise. Therefore, the baseband equivalent of the total received signal at the receiver input can

be expressed as

$$r[n] = x_{\mathrm{D}}[n] + x_{\mathrm{TxL}}[n] + w[n] \tag{10}$$

where $x_{\mathrm{D}}[n]$ and $w[n]$ denote the RX signal and thermal noise at the RX input.

On the RX side, the presence of noncontiguous TX passband leakage signal, given by (5), can trigger nonlinearity of receiver front-end components. In the case when RX LNA has finite IIP3, the spurious IMD products of the TX passband leakage signal also then appear at the IM sub-bands. The baseband equivalent output of the LNA can now be written as

$$\begin{aligned} r_{\mathrm{LNA}}[n] =& f_1^{\mathrm{LNA}}[n] \star r[n] + \sum_{\substack{l=3 \\ l\ odd}}^{L} f_l^{\mathrm{LNA}}[n] \star \left(|r[n]|^{l-1}\, r[n] \right) \\ \approx& f_1^{\mathrm{LNA}}[n] \star x_{\mathrm{D}}[n] + f_1^{\mathrm{LNA}}[n] \star x_{\mathrm{TxL}}[n] + \\ & f_1^{\mathrm{LNA}}[n] \star w[n] + \\ & \sum_{\substack{l=3 \\ l\ odd}}^{L} f_l^{\mathrm{LNA}}[n] \star \left(|x_{\mathrm{TxL}}[n]|^{l-1}\, x_{\mathrm{TxL}}[n] \right). \end{aligned} \tag{11}$$

where the LNA nonlinearity is modeled with a memory polynomial, with $f_1^{\mathrm{LNA}}[n]$ denoting the LNA small signal response and $f_l^{\mathrm{LNA}}[n]$ characterizing the LNA nonlinear properties. Here, we ignore the cross modulation products between the received signal, the transmitter leakage signal, and the noise, as their powers are negligibly small when the received signal $x_{\mathrm{D}}[n]$ is weak.

In the receiver chain, the overall signal at the LNA output is then down-converted to the baseband and filtered by the channel selection filter (CSF). Thus, the received baseband signal is given by

$$r_{\mathrm{BB}}[n] = \bar{x}_{\mathrm{D}}[n] + \bar{w}_{\mathrm{BB}}[n] + \underbrace{x_{\mathrm{IMD}}^{\mathrm{PA}}[n] + x_{\mathrm{IMD}}^{\mathrm{LNA}}[n]}_{x_{\mathrm{IMD}}[n]} \tag{12}$$

where $h_{\mathrm{CSF}}[n]$ denotes the CSF response and

$$x_{\mathrm{IMD}}^{\mathrm{PA}}[n] = h_{\mathrm{CSF}}[n] \star f_1^{\mathrm{LNA}}[n] \star x_{\mathrm{TX}}^{\mathrm{OOB}}[n] e^{-j\Delta\omega n} \tag{13a}$$

$$\begin{aligned} x_{\mathrm{IMD}}^{\mathrm{LNA}}[n] =& h_{\mathrm{CSF}}[n] \star \\ & \sum_{\substack{l=3 \\ l\ odd}}^{L} f_l^{\mathrm{LNA,IM3_+}}[n] \star \left(|x_{\mathrm{TxL}}[n]|^{l-1}\, x_{\mathrm{TxL}}[n] \right) \end{aligned} \tag{13b}$$

and $\bar{x}_{\mathrm{D}}[n]$ and $\bar{w}_{\mathrm{BB}}[n]$ simply refer to the desired RX signal and thermal noise at the CSF output. From (12), two different sources of receiver in-band self-interference can be clearly observed, as written explicitly in (13a) and (13b). The third term $x_{\mathrm{IMD}}^{\mathrm{PA}}[n]$ in (12), as written in (13a), represents the PA nonlinearity-induced IMD leakage which, after duplexer isolation, is present in the RX band. The other undesired signal present in the RX band, $x_{\mathrm{IMD}}^{\mathrm{LNA}}[n]$ in (13b), is the receiver nonlinearity-induced IMD of the transmitter passband leakage signal. Although the latter interference is generally weaker than the PA nonlinearity-induced interference, it may still be substantial to degrade the RX signal-to-interference-plus-noise ratio (SINR) as was already demonstrated by the example system calculations in Section II.

Stemming from the above modeling and signal structures, we next develop an efficient receiver in-band self-interference regeneration technique in the transceiver digital front-end and its subsequent suppression. Furthermore, the needed parameter estimation methods are also discussed.

IV. Proposed RX In-band Self-Interference Regeneration and Cancellation Solution

The estimation and regeneration of the RX in-band self-interference are addressed in this section, and the corresponding cancellation method is devised. For the sake of compactness, we restrict our focus to the positive IM3 sub-band only and it is assumed that it lies in the RX operating band. The proposed solution, however, can be easily generalized to any IM sub-band with minor modifications, by using the basis functions given in (9), (A.2), (A.6), (A.7), (A.8).

The proposed receiver in-band self-interference regeneration and cancellation unit operates in the digital front-end of the FDD transceiver, as shown in Fig. 2. It also employs an *observation receiver* connected to the LNA input for the purpose of learning the TX passband leakage channel parameters. As we show in the following subsections, the proposed formulation results in a model which is linear in the parameters for the IMD present in own RX band, thus leading to a simple and efficient estimation and cancellation of the self-interference.

A. Modeling and Estimation of TX Passband Leakage Channel

In order to regenerate and cancel the self-interference, the transmitter passband leakage channel is first estimated from the received signal of the observation receiver. The local oscillator (LO) frequency in the observation receiver, observing the LNA input, is tuned to the TX center frequency, thus down-converting the TX passband leakage signal from RF to baseband, followed by filtering to remove the TX emissions outside the TX band.

Based on the earlier modeling in the previous section, in (5)-(7), the observed baseband signal from the observation receiver is given by

$$\begin{aligned} x_{\mathrm{RX}}^{\mathrm{OBS}}[n] =& h_{\mathrm{CSF}}^{\mathrm{OBS,RX}}[n] \star h_{\mathrm{D}}[n] \star \\ & \sum_{\substack{p=1 \\ p\ odd}}^{P} \begin{pmatrix} f_p^{\mathrm{PA,IF_+}}[n] \star \psi_p^{\mathrm{PA,IF_+}}[n] + \\ f_p^{\mathrm{PA,IF_-}}[n] \star \psi_p^{\mathrm{PA,IF_-}}[n] \end{pmatrix} \\ =& \sum_{\substack{p=1 \\ p\ odd}}^{P} h_p^{\mathrm{CC1}}[n] \star \bar{\psi}_p^{\mathrm{PA,IF_+}}[n] \\ & + \sum_{\substack{p=1 \\ p\ odd}}^{P} h_p^{\mathrm{CC2}}[n] \star \bar{\psi}_p^{\mathrm{PA,IF_-}}[n] + w_{\mathrm{RX}}^{\mathrm{OBS}}[n] \end{aligned} \tag{14}$$

where $h_p^{\mathrm{CC1}}[n] = h_{\mathrm{D}}[n] \star f_p^{\mathrm{PA,IF_+}}[n]$ and $h_p^{\mathrm{CC2}}[n] = h_{\mathrm{D}}[n] \star f_p^{\mathrm{PA,IF_-}}[n]$ denote the unknown TX passband leakage channels, modeling the duplexer filter response, PA gain, and the nonlinear PA with memory response on the p^{th} basis function of the transmit component carriers, while $\bar{\psi}_p^{\mathrm{PA,IF_{+;-}}}[n]$ are the

known basis functions for different PA nonlinearity orders, as given in (7), but being filtered by the observation RX CSF response $h_{\mathrm{CSF}}^{\mathrm{OBS,RX}}[n]$. The thermal noise in the observation receiver is denoted here by $w_{\mathrm{RX}}^{\mathrm{OBS}}[n]$.

The model in (14) is linear in the parameters $h_p^{\mathrm{CC1;2}}[n]$. Therefore, any standard estimator for linear signal models, such as linear least squares (LS) [25], can be used for the parameter estimation, while the basis functions, $\bar{\psi}_p^{\mathrm{PA,IF}_+}[n]$ in in (14), can be pre-calculated by utilizing the known transmit signal and the observation RX CSF impulse response. After estimating the TX passband leakage filters, a local replica of the TX passband leakage signal can be generated at the baseband. In the next subsection, this is utilized to estimate and regenerate the spurious IMD-induced receiver in-band self-interference, and thereafter its cancellation.

B. Overall Model of Joint TX and RX Nonlinearity Induced Self-Interference

After estimating the TX passband leakage signal, the overall self-interference can now be expressed as a model which is linear in the parameters. When the third-order IM sub-bands lies in the RX operating band, the spurious IMD term $x_{\mathrm{IMD}}[n]$, as given in (12), can be first equivalently re-expressed as

$$\begin{aligned} x_{\mathrm{IMD}}[n] =& x_{\mathrm{PA}}^{\mathrm{IM3}_+}[n] + x_{\mathrm{LNA}}^{\mathrm{IM3}_+}[n] \\ =& \sum_{\substack{k1=3 \\ k1\ odd}}^{K1} h_{k1}^{\mathrm{PA,IM3}_+}[n] \star \bar{\psi}_{k1}^{\mathrm{PA,IM3}_+}[n] \\ &+ \sum_{\substack{k2=3 \\ k2\ odd}}^{K2} f_{k2}^{\mathrm{LNA,IM3}_+}[n] \star \bar{\psi}_{k2}^{\mathrm{LNA,IM3}_+}[n] \\ &+ \sum_{\substack{k3=3 \\ k3\ odd}}^{K3} h_{k3}^{\mathrm{PA,LNA,IM3}_+}[n] \star \bar{\psi}_{k3}^{\mathrm{PA,LNA,IM3}_+}[n] \end{aligned} \tag{15}$$

where $h_{\mathrm{k}}^{\mathrm{PA,IM3}_+}[n]$, $f_k^{\mathrm{LNA,IM3}_+}[n]$ and $h_{\mathrm{k}}^{\mathrm{PA,LNA,IM3}_+}[n]$ denote the *unknown equivalent IM3$_+$ channel filters*, modeling the TX and RX nonlinearities present in the IM3$_+$ sub-band, and acting on the k^{th} basis function. On the other hand, the basis functions can be constructed using the known quantities such as the baseband CC signals $x_1[n]$ and $x_2[n]$, the estimated TX passband leakage signal, the known CSF response, and the frequency separation $\Delta\omega$, as

$$\begin{aligned} \bar{\psi}_{\mathrm{k}}^{\mathrm{PA,IM3}_+}[n] \triangleq& h_{CSF}[n] \star \left(\psi_k^{\mathrm{PA,IM3}_+}[n]\right) e^{-j\Delta\omega n} \\ \bar{\psi}_k^{\mathrm{LNA,IM3}_+}[n] \triangleq& h_{CSF}[n] \star \left(\psi_k^{\mathrm{LNA,IM3}_+}[n]\right) e^{-j\Delta\omega n} \\ \bar{\psi}_k^{\mathrm{PA,LNA,IM3}_+}[n] \triangleq& h_{CSF}[n] \star \\ & \left(\begin{array}{c} 2 \times \psi_k^{\mathrm{PA,IM3}_+}[n] \times \\ \left(|\hat{x}_1[n]|^2 + |\hat{x}_2[n]|^2\right) \end{array}\right) e^{-j\Delta\omega n}. \end{aligned} \tag{16}$$

Here, $\hat{x}_{1;2}[n] = \sum_{\substack{p=1 \\ p\ odd}}^{P} \hat{h}_p^{\mathrm{CC1;2}}[n] \star \psi_p^{\mathrm{IF}_{+;-}}[n]$ denote the estimates of the TX passband leaking CCs at the LNA input, and $\psi_k^{\mathrm{LNA,IM3}_+}[n]$ is of the same form as $\psi_k^{\mathrm{PA,IM3}_+}[n]$ but with the substitution $x_{1;2}[n] = \hat{x}_{1;2}[n]$.

The model in (15) is linear in the unknown parameters $h_k^{\mathrm{PA,IM3}_+}[n]$, $f_k^{\mathrm{LNA,IM3}_+}[n]$ and $h_k^{\mathrm{PA,LNA,IM3}_+}[n]$. Therefore, as previously, any standard estimator for linear signal models, such as linear LS [25], can be used for estimating them.

C. Regeneration and Cancellation

Once the parameters of the TX passband leakage channel and the equivalent IM3$_+$ channel filters are all estimated, they can be utilized together with the known parameters and quantities during the transceiver online operation to regenerate an accurate replica of the nonlinear self-interference. Formally, the regeneration is done using (15), written as

$$\begin{aligned} \hat{x}_{\mathrm{IMD}}[n] =& \hat{x}_{\mathrm{PA}}^{\mathrm{IM3}_+}[n] + \hat{x}_{\mathrm{LNA}}^{\mathrm{IM3}_+}[n] \\ =& \sum_{\substack{k1=3 \\ k1\ odd}}^{K1} \hat{h}_{k1}^{\mathrm{PA,IM3}_+}[n] \star \bar{\psi}_{k1}^{\mathrm{PA,IM3}_+}[n] \\ &+ \sum_{\substack{k2=3 \\ k2\ odd}}^{K2} \hat{f}_{k2}^{\mathrm{LNA,IM3}_+}[n] \star \bar{\psi}_{k2}^{\mathrm{LNA,IM3}_+}[n] \\ &+ \sum_{\substack{k3=3 \\ k3\ odd}}^{K3} \hat{h}_{k3}^{\mathrm{PA,LNA,IM3}_+}[n] \star \bar{\psi}_{k3}^{\mathrm{PA,LNA,IM3}_+}[n]. \end{aligned} \tag{17}$$

Here, the regenerated signals and the estimated variables are denoted with overscript $\hat{(\cdot)}$. It can be noticed from (17) that through direct substitution of the essential basis functions and the estimated parameters, both individually as well as coexisting TX and RX nonlinearity-induced self-interference can be flexibly regenerated. In particular, if only the PA induced self-interference is to be canceled, only the first term in the second line of (17) is executed while the rest are omitted.

To finally suppress the self-interference, the regenerated overall TX leakage in (17) is subtracted from the received signal in (12), expressed formally as

$$\hat{\tilde{x}}_{\mathrm{D}}[n] = r_{\mathrm{BB}}[n] - \hat{x}_{\mathrm{IMD}}[n]. \tag{18}$$

Thus, during the transceiver online operation, (17) and (18), together with the calculation of the associated basis function samples, need to be all executed in a sample-by-sample manner. The proposed overall self-interference regeneration and cancellation solution is summarized in Algorithm 1, and is also conceptually illustrated in Fig. 2.

In general, it is important to recognize that the observation receiver is needed only in the TX passband leakage channel parameter estimation phase, whereas the actual IM sub-band channel filters needed for the overall receiver in-band self-interference regeneration and cancellation are estimated directly from the device's main receiver observation. This, in turn, can be done either in a specific calibration period or even in the online mode, while receiving a useful signal, in which case the actual RX signal simply acts as noise in the parameter estimation process. Furthermore, since the proposed technique operates in the transceiver digital front-end where the real-time transmit data is always available during the cancellation phase,

Algorithm 1: Summary of the Overall Estimation, Regeneration and Cancellation Processing.

1) Parameter estimation
   - Estimate the TX passband leakage channel filter parameters $h_p^{\mathrm{CC1}}[n]$ and $h_p^{\mathrm{CC2}}[n]$ based on (7) and (14).
   - Estimate the IM sub-band channel filter parameters $h_{k1}^{\mathrm{PA,IM3}_+}[n]$, $f_{k2}^{\mathrm{LNA,IM3}_+}[n]$, and $h_{k1}^{\mathrm{PA,LNA,IM3}_+}[n]$ based on (9), (15), and (16).
2) Online regeneration and cancellation
   - Execute (17) on a sample-by-sample basis to regenerate the receiver in-band self-interference.
   - Based on (18), suppress the receiver in-band self-interference by subtracting it from the received signal.

all necessary synchronization functions, including the timing offset, can be straight-forwardly implemented. In addition, the self-interference cancellation can be done at the sample rate which is relative to the RX bandwidth only. In the next section, we discuss in greater details the sample rate and other computing and implementation related aspects.

V. Implementation Aspects

A. Complexity Analysis

One of the attractive features of the proposed receiver in-band self-interference regeneration and cancellation scheme is that it explicitly exploits the frequency-domain structure of the aggregated CCs to obtain an efficient processing method tailored for the specific IM sub-bands that are in the RX operating band. As a consequence, the involved computations in terms of the number of parameters needed for accurate modeling of the involved responses and the required processing sample rate can be relatively low.

In general, the minimum required sample rate for the TX passband leakage signal regeneration depends on the considered PA nonlinearity order, i.e., $f_s^{\mathrm{reg,TXpassband}} = P \times B_{\mathrm{TX}}$, where P denotes the maximum order of the IMD products considered in the TX leakage signal, and B_{TX} is the bandwidth of the individual TX CCs. For example, regenerating the TX passband leakage signal in which the IMD products of order up to 5 around the CCs are considered would require a minimum sample rate that is at least five times the CC bandwidth. On the other hand, the minimum sample rate for regenerating the self-interference at a specific IM sub-band depends on a number of factors, i.e., the gap between the center frequency of the IM sub-band and the center frequency of the desired received signal, the RX signal bandwidth, and the considered nonlinearity orders of the TX leakage signal. Formally, it can be quantified as [14]

$$f_s^{\mathrm{reg,IM}} = \max\left\{B_L + B_{\mathrm{RX}}, B_U + B_{\mathrm{RX}}\right\} \tag{19}$$

where B_U, B_L denote the IMD bandwidths above and below the RX signal bandwidth, respectively, while B_{RX} denotes the actual RX signal bandwidth. The above expression allows aliasing of the IMD products in the region that is outside the RX signal bandwidth. In the cases when the IM sub-band and the RX signal are both located on the same center frequency, then $f_s^{\mathrm{reg,IM}} = \left(\left(P+1\right)/2\right) B_{\mathrm{RX}}$.

TABLE II
Running complexities of the self-interference cancelers, assuming intraband noncontiguous CA transmission with Two 5 MHz CCs, fifth-order PA and third-order LNA models. The interference regeneration and cancellation sample rate is 15 MHz, and $N_1 = 5, N_2 = 3$.

	Basis function generation and filtering (FLOPs)	Self-interference regeneration and cancellation complexity (GFLOPS)
PA nonlinearity canceler	$16N_1 + 23$	1.55
Joint PA and LNA nonlinearity canceler	$16N_1 + 8N_2 + 29$	1.99

Moreover, the running computational complexity can be quantified by evaluating the floating point operations per second (FLOPS), and consists of two parts, namely the complexity of interference regeneration, and the subsequent interference cancellation. The interference regeneration complexity is further composed of the complexity of basis functions generation and filtering, defined in terms of floating point operations (FLOPs) per sample, and the complexity of actual interference regeneration operation, defined in terms of FLOPS. As shown in Fig. 2 and equation (18), the interference cancellation is a simple complex addition as we generate an opposite-phase replica of the undesired self-interference, thus requiring only 2 FLOPs [26].

Notice that, when aiming at a feasible running complexity, it is important to recognize that the PA-induced IMD leakage products are generally stronger then the RX LNA-induced IMD distortion. Therefore, one may consider to deploy a canceler where different orders of IMD products are considered for the PA and the LNA nonlinearity modeling, with PA nonlinearity canceler containing higher-order IMD products than the LNA-related nonlinearity canceler. This will eventually lead to a considerable complexity reduction. The proposed solution, described in (17), supports this flexibility to include arbitrary numbers of basis functions in the modeling and interference regeneration.

Now, to quantify the complexity of the proposed technique, we consider a practical case of intraband noncontiguous CA transmission. The transmit signal is composed of two CCs, each with 5 MHz bandwidth, and for simplicity, it is again assumed that the $\mathrm{IM3}_+$ sub-band is located at the same center frequency as the desired RX signal. Table II summarizes the required amounts of numerical operations for regenerating the PA-induced self-interference, and for joint PA and LNA-induced self-interference. Here, the channel filter lengths corresponding to a basis function are denoted by N_1, N_2 for the PA and LNA nonlinearity modeling, respectively. The minimum required sample rate for the receiver in-band self-interference regeneration can be easily calculated to be $f_s^{\mathrm{reg,IM}} = 15$ MHz. As shown in Table II, the computational complexity of the proposed joint PA and LNA nonlinearity canceler is slightly greater than the complexity of the PA

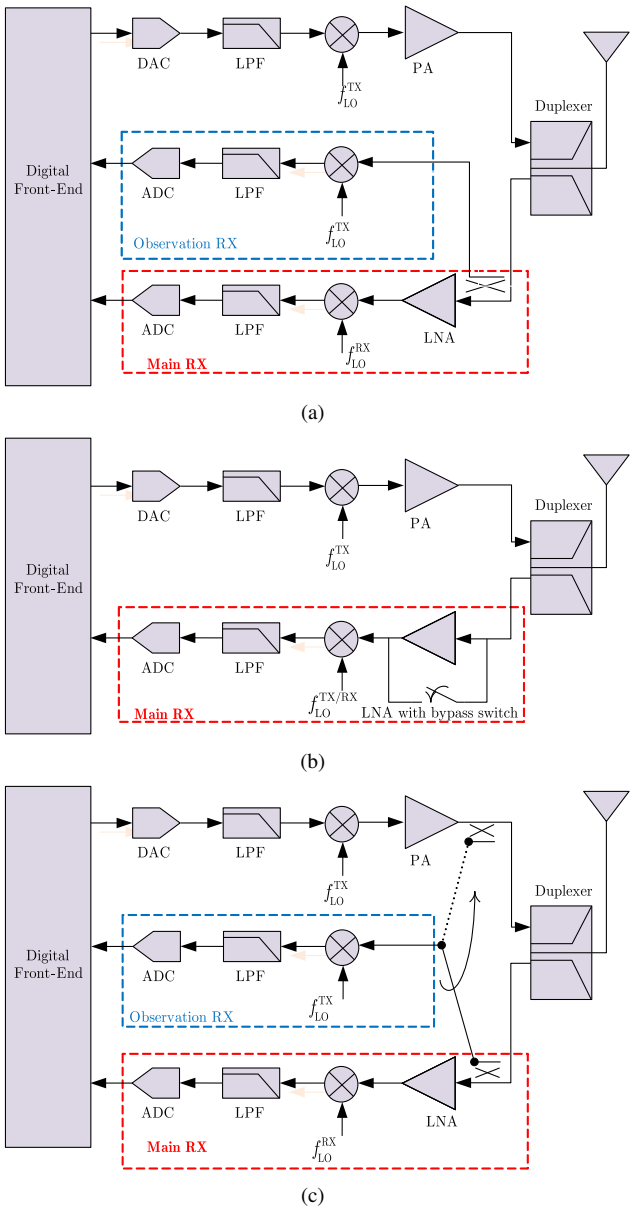

Fig. 3. Alternative architectures for implementing the observation receiver: (a) a dedicated observation receiver chain is employed to observe the TX passband leakage signal; (b) main receiver of the device is momentarily tuned for observing the TX passband leakage signal while the RX LNA is bypassed; (c) observation receiver chain in the TX is flexibly employed for either TX PA linearization or for sensing the TX passband leakage signal.

nonlinearity canceler. While the giga FLOPS (GFLOPS) processing may seem substantial, even in mobile devices with limited battery power, existing computing platforms can already support such processing requirements [27]. The purpose of this indicative example is only to show that the involved computing complexity is feasible, in particular in higher-power BS equipment already today, and potentially also in the longer run in mobile devices.

B. Observation Receiver Implementation Considerations

The proposed receiver in-band self-interference regeneration and cancellation solution builds on first estimating the TX passband leakage channel, in order to regenerate the TX passband signal leaking into the RX, followed by estimating the equivalent IM sub-band channel filters. During the parameter estimation of the TX passband leakage channel, an observation of the transmit signal leaking into the RX is required. In this section, we discuss and present three alternative approaches on how the observation receiver functionality can be implemented in practice.

The first architecture, shown in Fig. 3(a), employs a dedicated observation receiver chain connected to the LNA input, tuned to TX center frequency, which observes the TX passband leakage signal at the LNA input in order to separately estimate the TX passband leakage channel. Such an approach is very straight-forward but will, however, clearly increase the transceiver size and complexity, and thus may not be very appealing in particular for compact mobile devices.

The second architecture shown in Fig. 3(b) uses the device's main receiver for capturing the TX passband leakage signal. The idea here is to employ an LNA with a bypass switch in the RX chain, where the LNA is switched off in order to avoid LNA nonlinear distortion, and and the RX LO frequency is momentarily tuned to the TX frequency for the passband leakage channel estimation. While such an approach is indeed plausible with state-of-the-art LNA modules (*e.g.* NXP BGS8M4UK LNA), it naturally requires a separate calibration period where no actual RX signal can be received.

As a third alternative architecture, the observation receiver of the TX chain, used commonly for digital predistortion (DPD) parameter learning, can also be utilized for passband leakage channel estimation by switching its input to the LNA input, as shown in Fig. 3(c). Conventionally, an observation receiver connected to the PA output is employed in radio transmitters, for learning the direct or inverse PA nonlinearity models [24], or to cancel the PA noise present at the RX band [10], [12], or to facilitate ACLR measurements. However, here we are interested in the transmitter passband leakage signal at the RX input, and the estimation of the TX passband leakage channel, therefore, the observation receiver chain input is switched to the LNA input. Thus, if such PA output observation receiver is already available, it can be used also for the TX passband leakage channel estimation with very minor hardware modifications.

VI. Simulation Results and Analysis

A. Basic UE Transceiver Simulation Settings

The performance of the proposed estimation, regeneration, and cancellation technique is now evaluated through computer simulations. The baseband transmit signal is composed of two 10 MHz LTE-Advanced uplink SC-FDMA component carriers and the CC spacing is $\Delta_{\mathrm{CC}} = 44$ MHz. The subcarrier modulation is quadrature phase-shift keying (QPSK) modulation. The TX PA is modeled by a Wiener nonlinearity, meaning that the PA memory is modeled through a filter, with transfer function of the form $\left(1 + 0.3z^{-2}\right) / \left(1 - 0.2z^{-1}\right)$, followed by a static nonlinearity. The static nonlinearity is an elementary fifth-order polynomial whose parameters have been obtained from a practical mobile PA through measurements, with PA

gain, output IP3, and output 1-dB compression point being equal to 28 dB, +41 dBm, and +31 dBm, respectively. As opposed to the PH PA model assumed in the proposed receiver in-band self-interference cancellation algorithm development, the adoption of a Wiener PA model in the simulation is deliberate in order to better quantify the performance under a model mismatch. The duplexer TX and RX filters are also based on the measured data of a real mobile duplexer, with frequency-selective stopband attenuation in the order of $40-60$ dB at the TX-RX band and 2 dB insertion loss in the passband.

As a practical example, we assume that the positive IM3 sub-band lies in the RX band. The RX LNA is also assumed nonlinear with a gain of 15 dB, an out-of-band IIP3 $= -5$ dBm, and noise figure of 2 dB. The overall NF of the main RX is then only 2.5 dB, which is generally-speaking a very low number but is done deliberately in order to have a challenging reference noise floor against which the self-interference cancellation performance is then compared. Thus, the reference thermal noise power level, referred to the LNA input, is -111.5 dBm measured over 1 MHz bandwidth. On the other hand, the NF of the observation RX is 9 dB, and the thermal noise floor is at -105 dBm/MHz in the observation receiver. The bandwidth of the desired RX signal is 10 MHz, and is based on LTE-Advanced downlink OFDM(A) radio interface numerology with QPSK subcarrier modulation, and is assumed to be operating at the reference sensitivity level, i.e., -93.5 dBm [4]. The desired RX signal and noise are both present when estimating the equivalent IM3 channel filters. In the simulations, a fifth-order PA nonlinearity canceler and a third-order LNA nonlinearity canceler are employed. The processing sample rate during the parameter estimation, and also during the self-interference regeneration and cancellation, is $f_s = 30.72$ MHz, that is twice the basic sample rate for TX/RX component carriers. Furthermore, $80k$ samples are utilized for estimating the filter coefficients, and the filter lengths corresponding to basis functions for the PA nonlinearity modeling are set to $7-$taps and for the LNA nonlinearity modeling to $5-$taps.

B. Performance Metrics

The cancellation performance is quantified in terms of the obtained interference suppression, by plotting the power spectral density (PSD) curves, and also by evaluating the receiver in-band SINR against different transmit power levels. The SINR is defined as a ratio of the desired RX signal power within the channel bandwidth (P_{RX}) and the sum of the interference power ($P_{\mathrm{Interference}}$) and the thermal noise power (P_{Noise}) within the channel bandwidth, namely,

$$\mathrm{SINR}_{\mathrm{dB}} = 10\log_{10}\left(\frac{P_{\mathrm{RX}}}{P_{\mathrm{Interference}} + P_{\mathrm{Noise}}}\right). \qquad (20)$$

C. Obtained Cancellation Performance

Fig. 4 shows the PSD curves of the receiver in-band self-interference without digital cancellation, and with different digital cancellation methods, when the transmit power is +23 dBm. The desired RX signal and noise are also shown in the figure. The achieved self-interference suppression as well as the corresponding complexity are summarized in Table III. It can be noticed from the figure that under limited duplexer isolation, narrow duplex distance, and nonlinear TX and RX chain components, the nonlinear self-interference is very strong, and will heavily corrupt the reception. However, the proposed technique suppresses the self-interference below the receiver noise floor. It is interesting to notice that the PA-only nonlinearity canceler, proposed originally by the authors in [14], already gives substantial interference suppression, yet the residual interference is still significant. This is due to the fact that the PA nonlinearity-induced IMD leaking into the RX band is in this case, and also typically, stronger than the LNA nonlinearity-induced IMD, as was explained with the system

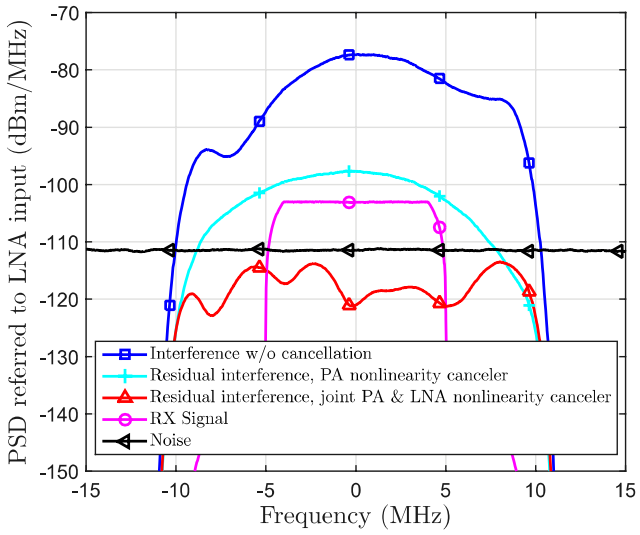

Fig. 4. Power spectra of the nonlinear receiver in-band self-interference with and without the digital cancellation, the desired RX signal, and the thermal noise. TX waveform is a noncontiguous CA LTE-Advanced uplink signal with two 10 MHz CCs and 44 MHz of frequency separation, and the desired received signal is 10 MHz LTE-Advanced downlink signal. TX power is +23 dBm, whereas RX signal is at the reference sensitivity level of -93.5 dBm.

TABLE III
COMPARISON OF SIMULATED SELF-INTERFERENCE SUPPRESSION. TX WAVEFORM IS A NONCONTIGUOUS CA LTE-ADVANCED UPLINK SIGNAL WITH TWO 10 MHZ CCS AND 44 MHZ OF FREQUENCY SEPARATION. THE TX POWER IS +23 DBM. THE RECEIVED SIGNAL IS A 10 MHZ OFDMA CARRIER, OPERATING AT -93.5 DBM LEVEL, WHEREAS THE THERMAL NOISE POWER IS -101.4 DBM. THE POWERS ARE REFERRED TO THE LNA INPUT.

	Power (dBm)	SINR (dB)	Complexity (GFLOPS)
self-interference without cancellation	-69.4	-23	N/A
self-interference with PA nonlinearity canceler	-89.2	-4.7	4.15
self-interference with joint PA and LNA nonlinearity canceler	-107.7	7.2	5.56

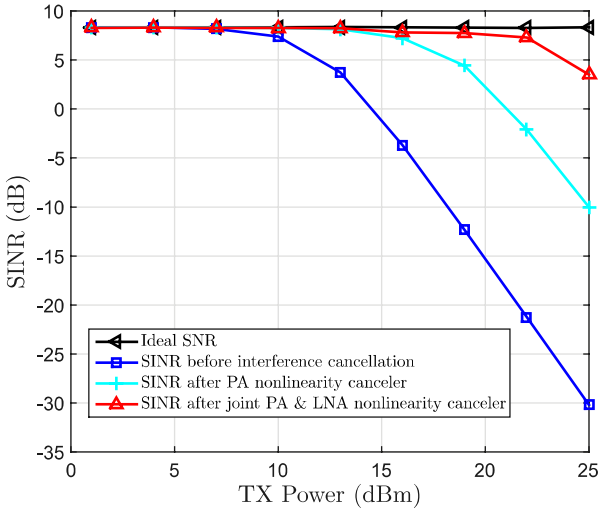

Fig. 5. Illustration of own RX SINR against different transmit power levels, with and without the nonlinear self-interference cancellation. TX waveform is a noncontiguous CA LTE-Advanced uplink signal with two 10 MHz CCs and 44 MHz of frequency separation, and the RX signal is a 10 MHz LTE-Advanced downlink signal. While the TX power is varying, the desired RX signal power is fixed at the reference sensitivity level of -93.5 dBm.

calculations already in Section II. However, only the proposed joint PA and LNA IMD canceler suppresses the interference fully below the noise floor, hence effectively mitigating the overall self-interference.

The receiver in-band SINR is next evaluated at various transmit power levels, and the obtained curves are plotted in Fig. 5. The degradation caused by the receiver in-band self-interference, and the corresponding improvement in enhancing the RX SINR through the proposed technique is clearly visible, showing that when the transmit power is increased beyond $+12$ dBm, the self-interference begins to deteriorate the achievable SINR. Assuming a target SINR of 5 dB, the PA nonlinearity canceler is capable of effectively suppressing the nonlinear receiver in-band self-interference for the TX powers up to $+17$ dBm in spite of a nonlinear RX LNA. This is because the TX passband signal leaking into the RX is still sufficiently weak such that the LNA is operating effectively in its linear region. However, for the TX powers greater than $+17$ dBm, the LNA nonlinearity starts to limit the cancellation performance. The proposed joint PA and LNA nonlinearity canceler is then able to reduce the nonlinear receiver in-band self-interference and thus improve the SINR of the receiver, even at the higher end of the adopted TX powers. Considering a typical $+23$ dBm transmit power level for an LTE/LTE-Advanced mobile transmitter, the proposed joint PA and LNA nonlinearity canceler enhances the RX SINR by more than 30 dB.

VII. Experimental RF Measurement Results

In this section, we report the results of practical RF measurements carried out using commercial PA, duplexer, and LNA modules for both UE and BS FDD transceivers, demonstrating the applicability of the proposed techniques in real-world transmission and reception scenarios. The measurement setup is composed of a National Instrument (NI) PXIe-5645R vector signal transceiver, containing both vector signal generator (VSG) and vector signal analyzer (VSA), to generate the TX and RX signals, and commercial LTE/LTE-Advanced PA, duplexer filter, and LNA modules. The vector signal transceiver samples the signal at 120 MHz sample rate, and the integrated receiver in VSA, which has 80 MHz instantaneous capture bandwidth, is used for down-conversion and digitization of the received signal. A host processor equipped with MATLAB is adopted for carrying out the DSP-related tasks, as well as to control all the measurement instruments. The block diagram of the overall measurement setup is shown in Fig. 6(a) .

In the measurements, the time alignment of the measured received signal with the reference transmit data is critical for the efficient estimation of the cancellation parameters and thereby subsequent self-interference cancellation. The timing offset estimation, carried out in the digital baseband, is implemented in two phases. The first phase is the coarse timing offset estimation, which is accomplished by taking the peak value of the cross-correlation between the reference transmit data and the measured signal. The measured signal is then adjusted by the corresponding estimated time offset. In the next phase, we carry out fine synchronization that is based on Lagrange interpolation. Here, a third-order polynomial is fitted around the maximum of the cross-correlation function, and the peak of this polynomial is assumed as the true time alignment for the self-interference.

A. User Equipment Measurement Examples

We first evaluate the performance of the proposed self-interference cancellation scheme using commercial LTE/LTE-Advanced Band 25 (downlink: $1930-1995$ MHz, uplink: $1850-1915$ MHz) PA and duplexer filter modules for mobile terminals, as shown in Fig. 6(b). The PA in the TX chain (model no. ACMP-5002-TR1) has gain and $1-$dB compression point of 28 dB and $+31$ dBm, respectively, whereas the duplexer (model no. TQQ2504) has stopband attenuation in the order of $50\cdots60$ dB at the TX and RX bands. The baseband transmit signal is composed of two 5 MHz LTE-Advanced uplink SC-FDMA component carriers with QPSK modulation. The carrier spacing is 44 MHz, and the peak-to-average power ratio (PAPR) is 9 dB. The TX center frequency is 1.875 GHz. The IM3_+ sub-band is then located at 1.941 GHz, and the RX is assumed to be operating at the same carrier frequency. The desired received signal is an LTE-Advanced downlink OFDM(A) signal with 5 MHz carrier bandwidth, and is operating at -83.5 dBm, which is fed through the antenna connector of the duplexer. A wideband LNA in the RX chain (model no. HD24089) is adopted, which has 22 dB gain, 2 dB noise figure, and out-of-band $\text{IIP3} = -7$ dBm. The receiver in-band self-interference regeneration and cancellation processing sampling rate is 30 MHz, and a block of $80k$ samples is used for the estimation of TX passband leakage channel and the IM3_+ channel filters. The filter lengths for

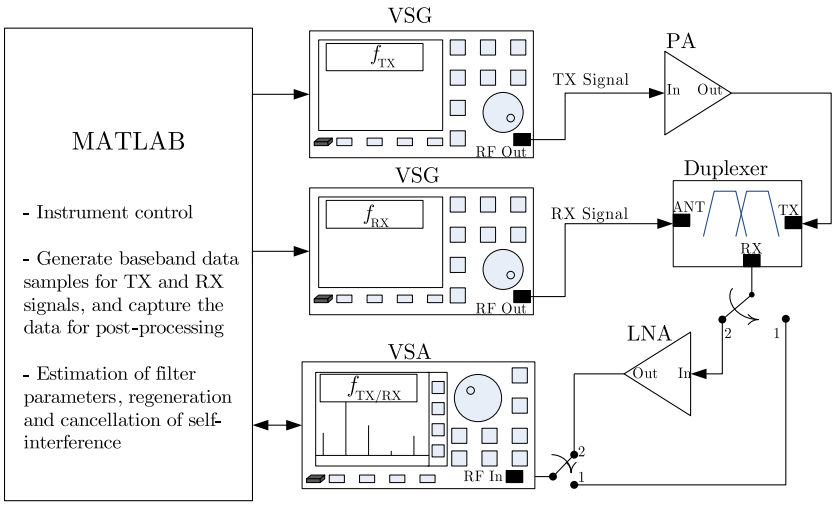

(a) Block diagram of the measurement setup

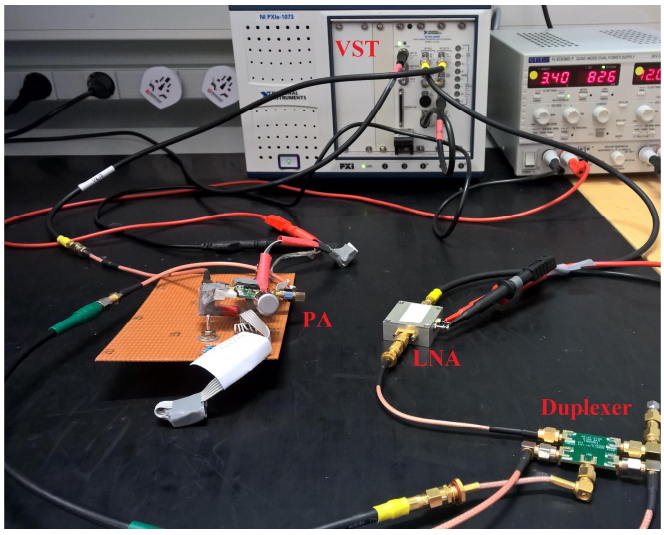

(b) UE RF measurements setup

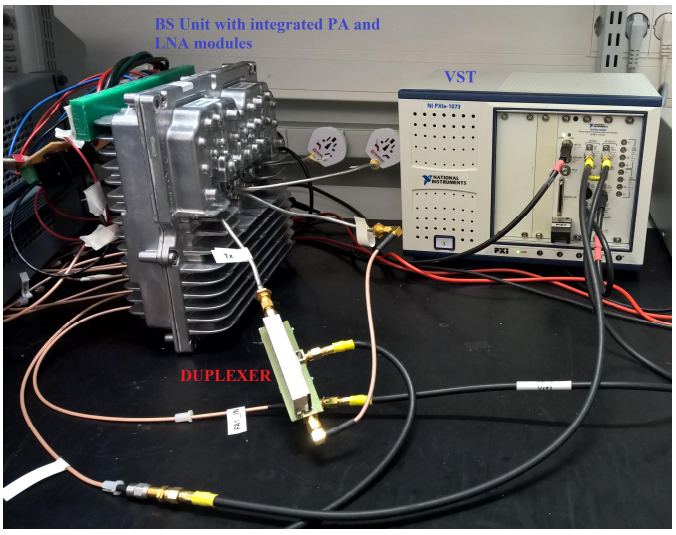

(c) BS RF measurements setup

Fig. 6. Experimental RF hardware setup for assessing and demonstrating the performance of the proposed receiver in-band self-interference cancellation algorithms. The LNA is bypassed during the TX passband leakage channel estimation.

PA and LNA nonlinearity modeling are 5−taps and 3−taps per basis function, respectively. Furthermore, a seventh-order PA-only canceler, which is an extension of [14], and a third-order LNA nonlinearity canceler are adopted here.

Fig. 7 shows the LNA input-referred spectra of the measured self-interference, with and without the digital cancellation, and the performance measures are also reported in Table IV. The transmit power, evaluated at the antenna port, is +23 dBm. This measurement result indicates that the relative strength of self-interference, without cancellation, is indeed substantial, and can fully desensitize the RX. The PA nonlinearity canceler provides significant interference suppression of up to 20 dB, again confirming that the PA nonlinearity is the major contributor in the overall receiver in-band self-interference. However, the residual self-interference after the PA nonlinearity cancellation is still strongly masking the desired RX signal. The proposed joint PA and LNA nonlinearity canceler then further pushes down the receiver in-band self-interference and enhances the RX SINR substantially.

TABLE IV
COMPARISON OF MEASURED SELF-INTERFERENCE SUPPRESSION AT +23 dBm TX POWER FOR UE UPLINK TRANSMISSION SCENARIO. THE DESIRED RX SIGNAL POWER IS −83.5 dBm, AND THE THERMAL NOISE POWER IS −95.2 dBm. THE POWERS ARE REFERRED TO THE LNA INPUT.

	Power (dBm)	SINR (dB)	Complexity (GFLOPS)
self-interference without cancellation	−63	−20.5	N/A
self-interference with PA nonlinearity canceler	−82.7	−0.8	4.59
self-interference with joint PA and LNA nonlinearity canceler	−88.3	4.8	5.49

Next, we carry out the SINR measurements for different transmit powers, with the desired RX signal power being fixed at −83.5 dBm, and the measured receiver in-band SINR curves

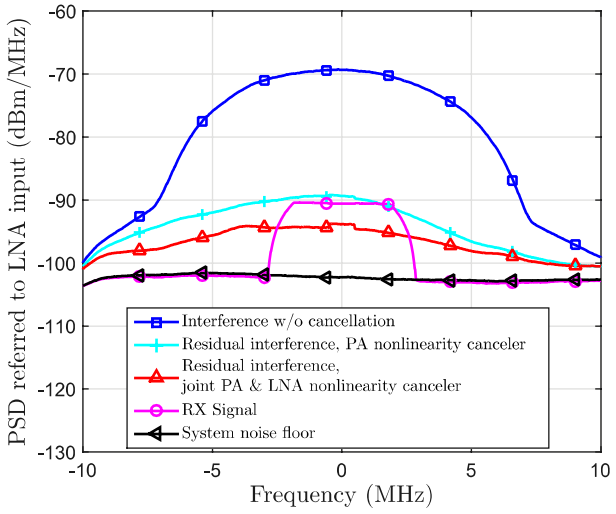

Fig. 7. Measured power spectra of the nonlinear self-interference in the UE uplink transmission scenario. TX waveform is CA LTE-Advanced uplink signal with two 5 MHz noncontiguous CCs and carrier spacing of 44 MHz, and the RX signal is a 5 MHz LTE-Advanced downlink signal. TX power is +23 dBm, and the RX signal power is −83.5 dBm.

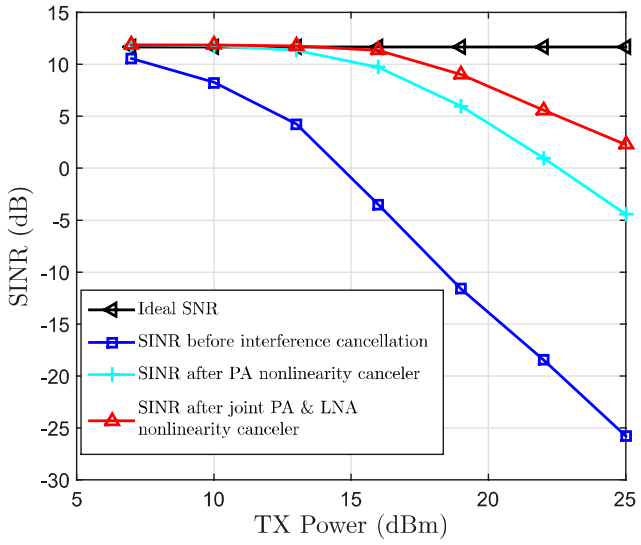

Fig. 8. Measured own RX SINR versus transmit powers, before and after self-interference cancellation in the UE uplink transmission scenario. TX signal is a CA LTE-Advanced uplink signal with two 5 MHz noncontiguous CCs and carrier spacing of 44 MHz, and the RX signal is an LTE-Advanced downlink signal with 5 MHz bandwidth. The RX signal power is being fixed at −83.5 dBm.

are plotted in Fig. 8, showing the significant performance improvement that can be obtained with the proposed technique. Notice that the isolation provided by state-of-the art duplexer module is clearly not sufficient, as for the transmit powers greater than +10 dBm, the self-interference starts to become powerful. The PA nonlinearity canceler improves the usable transmit power range, but at higher transmit power levels,

TABLE V
COMPARISON OF MEASURED RECEIVER IN-BAND SELF-INTERFERENCE SUPPRESSION AT +35 dBm TX POWER FOR BS DOWNLINK TRANSMISSION SCENARIO. THE DESIRED RX SIGNAL POWER IS −95 dBm, WHEREAS THE THERMAL NOISE POWER IS −100.5 dBm. THE POWERS ARE REFERRED TO THE LNA INPUT.

	Power (dBm)	SINR (dB)	Complexity (GFLOPS)
self-interference without cancellation	−85.5	−9.5	N/A
self-interference with PA nonlinearity canceler	−99.1	4.1	2.52

the LNA-induced nonlinear distortion starts to grow and limit the PA nonlinearity canceler suppression. The proposed joint PA and LNA nonlinearity canceler provides an additional 7 dB suppression compared to the PA nonlinearity canceler by giving at best up to 28 dB of the measured receiver in-band self-interference suppression, and further extending the usable transmit power range by about 3 dB compared to the PA nonlinearity canceler.

B. Base Station Measurement Examples

Next, we evaluate the performance using LTE Band 1 (downlink: 2110-2170 MHz, uplink:1920-1980 MHz) base station transceiver RF components, as shown in Fig. 6(c), adopting an LTE-Advanced BS PA (model no. MD7IC2250GN) with 31 dB gain and +47 dBm 1−dB compression point, duplexer filter with frequency-selective $65-70$ dB attenuation, and an LNA (model no. MGA-14516) with out-of-band IIP3 $=0$ dBm. Here, the baseband transmit signal is composed of two 1.4 MHz LTE-Advanced downlink OFDMA component carriers with carrier spacing of 50 MHz, and an aggregated baseband/IF sample rate of 120 MHz. The PAPR is 11 dB, and the TX center frequency is 2.14 GHz. In such carrier configuration, the negative IM7 sub-band (IM7$_-$) is then located at 1.965 GHz, which is here assumed to be the operating band of the own RX. The desired RX signal is a 1.4 MHz LTE/LTE-Advanced uplink SC-FDMA signal, operating at −95 dBm and being injected into the antenna port of the duplexer. The sampling rate for regeneration and cancellation processing is $f_s = 24$ MHz and a block of $80k$ samples is used for the estimation of TX passband leakage channel and the IM7$_-$ channel filters. The filter length corresponding to each basis function is again 3−taps. Here, we now adopt an eleventh-order PA nonlinearity canceler and a seventh-order LNA nonlinearity canceler. We note that while LTE Band 1 does not strictly-speaking support noncontiguous intraband CA in commercial networks, at least so far, it is used here as an indicative example representing an elementary proof-of-concept.

Fig. 9 shows the LNA input-referred power spectra curves of the measured nonlinear receiver in-band self-interference, with and without the proposed digital cancellation, and the measured powers are also summarized in Table V. The actual TX power, evaluated at the antenna port of the duplexer, is +35 dBm. This measurement result indicates that the

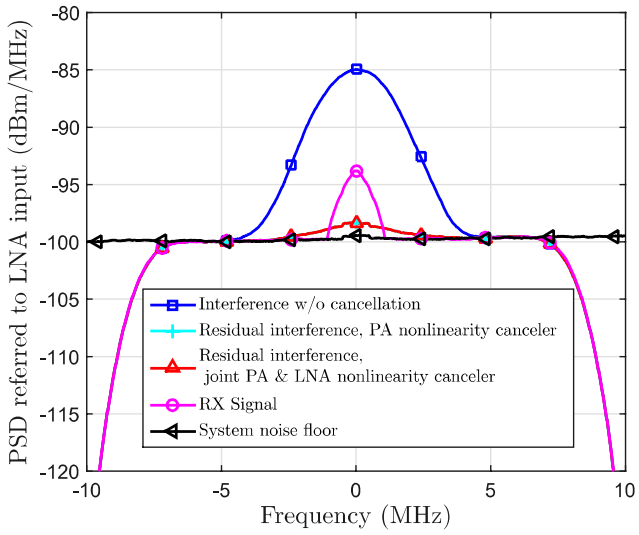

Fig. 9. Measured power spectra of the nonlinear receiver in-band self-interference in the BS downlink transmission scenario. TX signal is a CA LTE-Advanced downlink signal with two 1.4 MHz noncontiguous CCs and carrier spacing of 50 MHz, and the RX signal is a 1.4 MHz LTE-Advanced uplink signal. TX power is $+35$ dBm, whereas the RX signal power is -95 dBm.

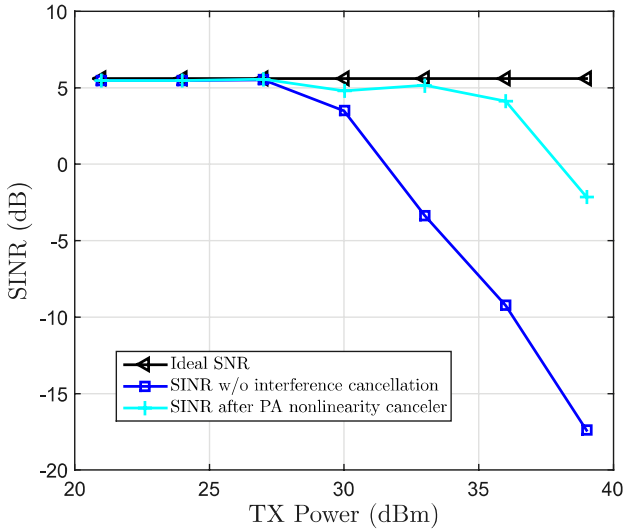

Fig. 10. Measured own RX SINR versus transmit powers, before and after the receiver in-band self-interference cancellation in the BS downlink transmission scenario. TX signal is a CA LTE-Advanced downlink signal with two 1.4 MHz noncontiguous CCs and carrier spacing of 50 MHz, and the RX signal is a 1.4 MHz LTE-Advanced uplink signal. The RX signal power is being fixed here at -95 dBm.

relative strength of the spurious IMD interference appearing in the RX band can still be significant with practical duplexer isolation, even when the duplex gap is significantly large, as in this example. This aspect has generally been ignored in the existing literature, however the presence of such strong self-interference can indeed reduce the RX sensitivity, particularly if it is operating close to the reference sensitivity level. The eleventh-order PA nonlinearity canceler, proposed in this paper, is able to push the receiver in-band self-interference close to the noise floor, whereas the joint PA and LNA nonlinearity canceler does not provide any notable additional suppression in this case. The latter conclusion is logical because the LNA-induced IMD at the IM7 sub-band is sufficiently weak and does not cause any observable IMD in the own RX band.

In the final measurement example, we evaluate the SINR within the 1.4 MHz RX bandwidth as a function of the transmit power, with the desired RX signal power being fixed at -95 dBm, and the measured curves are plotted in Fig. 10. The obtained results demonstrate the excellent receiver in-band self-interference suppression properties of the proposed technique in the practical BS transmission and reception scenarios. It can be noticed that the PA nonlinearity canceler extends the usable transmit power range by up to 6 dB, and provides an interference suppression of up to 14 dB, despite a large duplex distance at Band 1.

C. Further Discussion

As can be seen from the reported measurement results in Figs. 7 - 10, there is still some residual receiver in-band self-interference that the proposed canceler cannot fully mitigate. This can be attributed to several potential errors in the measurement setup. The first aspect is the potential *model mismatch* between the PH or memory polynomial models, assumed in the proposed algorithm development, and the real-world PA and LNA modules utilized in the measurement experiments. In such cases, it is obvious that the proposed estimation and regeneration processing cannot exactly reproduce a perfectly accurate copy of the true nonlinear self-interference, leading to a limited interference suppression. Another factor that may limit the canceler performance is the presence of even-order intermodulation distortion components at the spurious IM sub-bands, as discussed in [16]. Furthermore, measurement noise and other different imperfections of the measurement hardware including analog-to-digital converter (ADC) non-idealities, nonlinear distortions occurring in the VSA RX, as well as the potential errors in time and/or frequency synchronization may all limit the obtainable cancellation performance. Nevertheless, the proposed technique still gives substantial performance improvement, giving confidence that novel digital cancellation techniques like the ones proposed in this paper can be adopted in modern radio transceivers using state-of-the-art RF components to enhance their performance.

VIII. Conclusion

A novel nonlinear estimation, regeneration, and cancellation procedure was proposed in this paper, particularly tailored to noncontiguous CA FDD transceivers, to effectively reduce the receiver in-band self-interference, under coexisting nonlinear TX-RX front-end components. Compared to the existing methods, our formulations and processing solutions support higher-order IMD products as well as higher-order IM sub-bands, to provide a flexible and high-performance cancellation technique for mitigating the self-interference at arbitrary IM sub-bands

located in the RX operating band. The proposed parameter estimation solution, operating in two steps, first estimates the leakage channel response over the TX passband through an observation receiver chain, in order to model the TX passband leakage signal at the RX input. In the next step, the parameters of the sub-band channel filters, modeling the duplexer filter responses, nonlinear PA with memory, and LNA nonlinearity at the RX band, are estimated. The self-interference is then regenerated using the estimated nonlinear leakage channel parameters and the original online transmit data. The regenerated nonlinear self-interference is finally subtracted from the received signal. The simulation and experimental RF measurement results show promising performance, indicating up to 28 dB of measured receiver in-band self-interference suppression under realistic conditions. Hence, the proposed solutions can efficiently reduce the receiver desensitization problem, potentially relaxing the linearity requirements in CA-based flexible radio spectrum utilization and flexible duplexing in LTE-Advanced and emerging 5G radio systems.

APPENDIX
SPURIOUS IMD PRODUCTS AT HIGHER-ORDER IM SUB-BANDS

As discussed earlier in Section II, and demonstrated through RF measurements in Section VII, there are higher-order IM sub-bands such as IM5, IM7, IM9, etc., that can also lie within the RX band. We now present the exact expressions for the TX spurious IMD leakage signal at higher than third-order IM sub-bands. Starting with the spurious IM5 sub-band, the self-interference leaking into the RX chain can be expressed as

$$x_{\mathrm{TX}}^{\mathrm{OOB,IM5_+}}[n] = h_{\mathrm{D}}[n] \star \sum_{\substack{p=5 \\ p\ odd}}^{P} f_p^{\mathrm{PA,IM5_+}}[n] \star \psi_p^{\mathrm{PA,IM5_+}}[n] \tag{A.1}$$

where the basis functions at the $\mathrm{IM5}_+$ sub-band read

$$\begin{aligned}
\psi_5^{\mathrm{PA,IM5_+}}[n] &= x_1^3[n]\left(x_2^2[n]\right)^* \\
\psi_7^{\mathrm{PA,IM5_+}}[n] &= \psi_5^{\mathrm{PA,IM5_+}}[n] \times \left(3\left|x_1[n]\right|^2 + 4\left|x_2[n]\right|^2\right) \\
\psi_9^{\mathrm{PA,IM5_+}}[n] &= \psi_5^{\mathrm{PA,IM5_+}}[n] \times \begin{pmatrix} 6\left|x_1[n]\right|^4 + 10\left|x_2[n]\right|^4 + \\ 20\left|x_1[n]\right|^2\left|x_2[n]\right|^2 \end{pmatrix} \\
\psi_{11}^{\mathrm{PA,IM5_+}}[n] &= \psi_5^{\mathrm{PA,IM5_+}}[n] \times \begin{pmatrix} 10\left|x_1[n]\right|^6 + 20\left|x_2[n]\right|^6 + \\ 60\left|x_1[n]\right|^4\left|x_2[n]\right|^2 + \\ 75\left|x_1[n]\right|^2\left|x_2[n]\right|^4 \end{pmatrix}.
\end{aligned} \tag{A.2}$$

Similarly, the baseband equivalent spurious IMD leakage at the positive IM7, IM9, and IM11 sub-bands can be expressed as

$$x_{\mathrm{TX}}^{\mathrm{OOB,IM7_+}}[n] = h_{\mathrm{D}}[n] \star \sum_{\substack{p=7 \\ p\ odd}}^{P} f_p^{\mathrm{PA,IM7_+}}[n] \star \psi_p^{\mathrm{PA,IM7_+}}[n] \tag{A.3}$$

$$x_{\mathrm{TX}}^{\mathrm{OOB,IM9_+}}[n] = h_{\mathrm{D}}[n] \star \sum_{\substack{p=9 \\ p\ odd}}^{P} f_p^{\mathrm{PA,IM9_+}}[n] \star \psi_p^{\mathrm{PA,IM9_+}}[n] \tag{A.4}$$

$$x_{\mathrm{TX}}^{\mathrm{OOB,IM11_+}}[n] = h_{\mathrm{D}}[n] \star \sum_{\substack{p=11 \\ p\ odd}}^{P} f_p^{\mathrm{PA,IM11_+}}[n] \star \psi_p^{\mathrm{PA,IM11_+}}[n] \tag{A.5}$$

The corresponding SNL basis functions are given as

$$\begin{aligned}
\psi_7^{\mathrm{PA,IM7_+}}[n] &= x_1^4[n]\left(x_2^3[n]\right)^* \\
\psi_9^{\mathrm{PA,IM7_+}}[n] &= \psi_7^{\mathrm{PA,IM7_+}}[n] \times \left(4\left|x_1[n]\right|^2 + 5\left|x_2[n]\right|^2\right) \\
\psi_{11}^{\mathrm{PA,IM7_+}}[n] &= \psi_7^{\mathrm{PA,IM7_+}}[n] \times \begin{pmatrix} 10\left|x_1[n]\right|^4 + 15\left|x_2[n]\right|^4 + \\ 30\left|x_1[n]\right|^2\left|x_2[n]\right|^2 \end{pmatrix}
\end{aligned} \tag{A.6}$$

$$\begin{aligned}
\psi_9^{\mathrm{PA,IM9_+}}[n] &= x_1^5[n]\left(x_2^4[n]\right)^* \\
\psi_{11}^{\mathrm{PA,IM9_+}}[n] &= \psi_9^{\mathrm{PA,IM9_+}}[n] \times \left(5\left|x_1[n]\right|^2 + 6\left|x_2[n]\right|^2\right)
\end{aligned} \tag{A.7}$$

$$\psi_{11}^{\mathrm{PA,IM11_+}}[n] = x_1^6[n]\left(x_2^5[n]\right)^*. \tag{A.8}$$

Notice that while we have only considered the positive IM sub-bands in the above formulations, the corresponding expressions for the negative IM sub-bands can easily be obtained by interchanging $x_1[n]$ and $x_2[n]$ in the above equations. Furthermore, these basis functions can also easily be generalized for the LNA-induced IMD, through the substitution $x_{1;2}[n] \leftarrow \hat{x}_{1;2}[n]$, where $\hat{x}_{1;2}[n]$ is the estimated TX passband leakage CC at the LNA input. Finally, these basis functions can then be used in (15) and (16) to estimate the IM sub-band channel filters, and subsequently in (17) to regenerate the receiver in-band self-interference at IM sub-bands. Thus, through fairly simple substitutions of the involved basis functions, the proposed technique can flexibly model and cancel the self-interference at different IM sub-bands appearing in the RX operating band. This was also successfully demonstrated in Section VII-B, in terms of the $\mathrm{IM7}_-$ sub-band.

REFERENCES

[1] "Further advancements for E-UTRA physical layer aspects, " 3GPP, Tech. Rep. 36.814, version 9.0.0, Release 9, March 2010.

[2] M. Iwamura, K. Etemad, M. H. Fong, and R. Nory, "Carrier aggregation framework in 3GPP LTE-Advanced," *IEEE Commun. Mag.*, vol. 48, no. 8, pp. 60-67, August 2010.

[3] C. S. Park, L. Sundström, A. Wallen, and A. Khayallah, "Carrier aggregation for LTE-Advanced: design challenges of terminals," *IEEE Commun. Mag.,* vol. 51, no. 12, pp. 76-84, Dec. 2013.

[4] "Evolved Universal Terrestrial Radio Access (E-UTRA);User Equipment (UE) radio transmission and reception," 3GPP, Tech. Spec. 36.101, Release 14, Version 14.1.0, Sept. 2016.

[5] "R4-126964: REFSENS with one UL carrier for NC intra-band CA," Ericsson and ST-Ericsson, New Orleans, LA, USA, 2012.

[6] "R4-123797, UE reference sensitivity requirements with two UL carriers," Ericsson and ST-Ericsson, Qingdao, China, 2012.

[7] A. Frotzscher and G. Fettweis, "Digital compensation of transmitter leakage in FDD zero-IF receivers," *Trans. Emerging Telecommun. Techn.,* vol. 23, no. 2, pp. 105-120, March 2012.

[8] C. Lederer and M. Huemer, "Simplified complex LMS algorithm for the cancellation of second-order TX intermodulation distortions in homodyne receivers," in Proc. 45^{th} *Asilomar Conf. Signals, Syst. and Comput. (ASILOMAR)*, pp. 533-537, Nov. 2011.

[9] A. Kiayani, L. Anttila, and M. Valkama, "Modeling and dynamic cancellation of TX-RX leakage in FDD transceivers," in Proc. *IEEE* 56^{th} *International Midwest Symposium on Circuits and Systems (MWSCAS),* pp. 1089-1094, Aug. 2013.

[10] M. Omer, R. Rimini, P. Heidmann, and J. S. Kenney, "A compensation scheme to allow full duplex operation in the presence of highly nonlinear microwave components for 4G systems," in Proc. *IEEE MTT-S Int. Microwave Symp. Dig.*, pp. 1-4., June 2011.

[11] A. Kiayani, L. Anttila, and M. Valkama, "Digital suppression of power amplifier spurious emissions at receiver band in FDD transceivers," *IEEE Signal Process. Lett.,* vol. 21, no. 1, pp. 69-73, Jan. 2014.

[12] H. Gheidi, S. Farsi, Y. Liu, H. Dabag, P. Gudem, and P. M. Asbeck, "Digital signal injection technique for cancellation of receive-band spurious emissions in FDD cellular transmitters," in Proc. *IEEE MTT-S International Microwave Symposium (IMS)*, pp. 1-4, May 2015.

[13] A. Kiayani, M. Abdelaziz, L. Anttila, V. Lehtinen, and M. Valkama, "DSP-based suppression of spurious emissions at RX band in carrier aggregation FDD transceivers," in Proc. *22nd Eur. Signal Process. Conf.,* pp. 591-595, Sep. 2014.

[14] A. Kiayani, M. Abdelaziz, L. Anttila, V. Lehtinen, and M. Valkama, "Digital mitigation of transmitter-induced receiver desensitization in carrier aggregation FDD transceivers," *IEEE Trans. Microw. Theory Techn.,* vol. 63, no. 11, pp. 3608-3623, Dec. 2015.

[15] C. Yu, W. Cao, Y. Guo, and A. Zhu, "Digital compensation for transmitter leakage in non-contiguous carrier aggregation applications with FPGA implementation," *IEEE Trans. Microw. Theory Techn.,* vol. 64, no. 12, pp. 4306-4318, Dec. 2015.

[16] S. Farsi, H. Gheidi, H. T. Dabag, P. S. Gudem, D. Schreurs, and P. M. Asbeck, "Modeling of deterministic output emissions of power amplifiers into adjacent receive bands," *IEEE Trans. Microw. Theory Techn.,* vol. 63, no. 4, pp. 1250-1262, April 2015.

[17] H. T. Dabag, H. Gheidi, S. Farsi, P. S. Gudem, and P. M. Asbeck, "All-digital cancellation technique to mitigate receiver desensitization in uplink carrier aggregation in cellular handsets," *IEEE Trans. Microw. Theory Techn.,* vol. 61, no. 12, pp. 4754-4765, Dec. 2013.

[18] H. Gheidi, H. T. Dabag, Y. Liu, P. M. Asbeck, and P. Gudem, "Digital cancellation technique to mitigate receiver desensitization in cellular handsets operating in carrier aggregation mode with multiple uplinks and multiple downlinks," in Proc. *IEEE Radio Wireless Symp.,* pp. 221-224, Jan. 2015.

[19] "R1-166883, Discussion on flexible duplex operations in NR,", LG Electronics, 3GPP TSG RAN WG1 Meeting #86 ,Gothenburg, Sweden, 2016.

[20] S. A. Bassam, W. Chen, M. Helaoui, and F. M. Ghannouchi, "Transmitter architecture for CA: carrier aggregation in LTE-Advanced systems," *IEEE Microw. Mag.*, vol. 14, no. 5, pp. 78-86, July-Aug. 2013.

[21] "Radio Frequency (RF) system scenarios," 3GPP, Tech. Rep. 25.942, Release 12, Version 12.0.0, Oct. 2014.

[22] "Evolved Universal Terrestrial Radio Access (E-UTRA);Base Station (BS) conformance testing," 3GPP, Tech. Spec. 36.141, Release 14, Version 14.1.0, Sept. 2016.

[23] "Evolved Universal Terrestrial Radio Access (E-UTRA);Base Station (BS) radio transmission and reception," 3GPP, Tech. Spec. 36.104, Release 14, Version 14.1.0, Sept. 2016.

[24] M. Isaksson, D. Wisell, and D. Rönnow, "A comparative analysis of behavioral models for RF power amplifiers," *IEEE Trans. Microw. Theory Techn.,* vol. 54, no. 1, pp. 348-359, Jan. 2006.

[25] S. Haykin, *Adaptive Filter Theory*, 4^{th} ed. Upper Saddle River, NJ: Prentice-Hall, 2002.

[26] A. S. Tehrani, H. Cao, S. Afsardoost, T. Eriksson, M. Isaksson, and C. Fager, "A comparative analysis of the complexity/accuracy tradeoff in power amplifier behavioral models," *IEEE Trans. Microw. Theory Techn.,* vol. 58, no. 6, pp. 1510-1520, Jun. 2010.

[27] L. Codrescu, W. Anderson, S. Venkumanhanti, M. Zeng, E. Plondke, C. Koob, A. Ingle, C. Tabony, R. Maule,"Hexagon DSP: An architecture optimized for mobile multimedia and communications," *IEEE Micro*, vol. 34, no. 2, pp. 34-43, Mar. 2014.

Adnan Kiayani received the B.Sc. degree from COMSATS Institute of Information Technology, Pakistan, the M. Sc. (with honors) and Dr. Tech. degrees from Tampere University of Technology (TUT), Finland, in 2006, 2009 and 2015, all in electrical engineering. Since Jan. 2016, he has been a post-doctoral researcher at the Department of Electronics and Communications Engineering at TUT. His general research interests are in signal processing for communications and flexible radio transceivers. Currently, he is working on digital and RF cancellation techniques for self-interference suppression in simultaneous transmit and receive systems.

Lauri Anttila received the M.Sc. degree and D.Sc. (Tech) degree (with honors) in electrical engineering from Tampere University of Technology (TUT), Tampere, Finland, in 2004 and 2011. Currently, he is a Senior Research Fellow at the Department of Electronics and Communications Engineering at TUT. His research interests are in signal processing for wireless communications, radio implementation challenges in 5G cellular radio and full-duplex radio, flexible duplexing techniques, and transmitter and receiver linearization. He has co-authored over 70 peer reviewed articles in these areas, as well as two book chapters.

Marko Kosunen received his M.Sc, L.Sc and D.Sc (with honors) degrees from Helsinki University of Technology, Espoo, Finland, in 1998, 2001 and 2006, respectively. He is currently a Senior Researcher at Aalto University, Department of Electronics and Nanoengineering. His expertise is in implementation of the wireless transceiver DSP algorithms and communication circuits. He is currently working on implementations of digital intensive transceiver circuits and medical sensor electronics.

Kari Stadius received the M.Sc., Lic. Tech., and Doctor of Science degrees in electrical engineering from the Helsinki University of Technology, Helsinki, Finland, in 1994, 1997, and 2010, respectively. He is currently working as a staff scientist at the Department of Electronics and Nanoengineering, Aalto University School of Electrical Engineering. His research interests include the design and analysis of RF transceiver blocks with special emphasis on frequency synthesis. He has authored or coauthored over 70 refereed journal and conference papers in the areas of analog and RF circuit design.

Jussi Ryynänen was born in Ilmajoki, Finland, in 1973. He received his Master of Science, Licentiate of Science, and Doctor of Science degrees in electrical engineering from Helsinki University of Technology (HUT), Helsinki, Finland, in 1998, 2001, and 2004, respectively. He is currently working as an associate professor at the Department of Electronics and Nanoengineering, Aalto University School of Electrical Engineering. His main research interests are integrated transceiver circuits for wireless applications. He has authored or coauthored over 100 refereed journal and conference papers in the areas of analog and RF circuit design. He holds six patents on RF circuits

Mikko Valkama received his M.Sc. and Ph.D. degrees (both with honors) in electrical engineering from Tampere University of Technology (TUT), Finland, in 2000 and 2001, respectively. Currently, he is a Full Professor and Department vice-head at the Department of Electronics and Communications Engineering at TUT. His general research interests include communications signal processing, estimation and detection techniques, signal processing algorithms for flexible radio transmitters and receivers, cognitive radio, full-duplex radio, radio localization, 5G mobile cellular radio networks, digital transmission techniques such as different variants of multicarrier modulation methods and OFDM, and radio resource management for ad hoc and mobile networks.